Metallic 1T phase MoS₂ nanosheets as supercapacitor electrode materials

Muharrem Acerce, Damien Voiry and Manish Chhowalla*

Efficient intercalation of ions in layered materials forms the basis of electrochemical energy storage devices such as batteries and capacitors[1-6]. Recent research has focused on the exfoliation of layered materials and then restacking the two-dimensional exfoliated nanosheets to form electrodes with enhanced electrochemical response[7-11]. Here, we show that chemically exfoliated nanosheets of MoS₂ containing a high concentration of the metallic 1T phase can electrochemically intercalate ions such as H⁺, Li⁺, Na⁺ and K⁺ with extraordinary efficiency and achieve capacitance values ranging from ∼400 to ∼700 F cm⁻³ in a variety of aqueous electrolytes. We also demonstrate that this material is suitable for high-voltage (3.5 V) operation in non-aqueous organic electrolytes, showing prime volumetric energy and power density values, coulombic efficiencies in excess of 95%, and stability over 5,000 cycles. As we show by X-ray diffraction analysis, these favourable electrochemical properties of 1T MoS₂ layers are mainly a result of their hydrophilicity and high electrical conductivity, as well as the ability of the exfoliated layers to dynamically expand and intercalate the various ions.

High volumetric capacitances of ∼300 F cm⁻³ have been obtained with restacked graphene nanosheets[12,13]. Such high values are important for power sources in portable electronics. A new class of two-dimensional materials, the MXenes, are highly conducting and very hydrophilic, and have also recently shown promise as capacitors, with specific volumetric capacitances in excess of 900 F cm⁻³ (ref. 3).

Two-dimensional transition-metal dichalcogenides (2D TMDs) such as molybdenum disulphide (MoS₂) have been investigated for use in electrochemical storage[14-18]. MoS₂ has a 2H phase crystal structure (the coordination of its metal atoms is trigonal prismatic) with a monolayer bandgap of ∼1.9 eV, which renders it semi-insulating[19] and therefore not immediately attractive as an electrode material for energy storage. Indeed, only a few studies have described the electrochemical charge storage properties of electrodes consisting of single- and multi-layered MoS₂ nanosheets. To enhance the electrical conductivity, hybrid electrodes composed of graphene/MoS₂ (ref. 16) and polyaniline/MoS₂ (ref. 17) have been investigated. To date, however, the electrochemical storage performances (in terms of impedance and cyclability) obtained with either pure or hybrid 2H phase MoS₂ electrodes have been relatively modest compared with those of graphene[12,13] or MXene[3,8] electrodes. Our approach is to use the metallic 1T phase of MoS₂, which we have previously shown can be obtained from the semiconducting 2H phase of MoS₂ during chemical exfoliation of the bulk material[20]. The 1T MoS₂ phase is hydrophilic and 10⁷ times more conductive than the semiconducting 2H phase.

We used organolithium chemistry to exfoliate bulk MoS₂ powders into monolayer nanosheets with a 1T phase concentration of ∼70%, and obtained 100% monolayered MoS₂ nanosheets suspended in water using this well-established exfoliation method (see

Supplementary Fig. 3 for a photoluminescence spectrum confirming that the nanosheets are monolayered)[20]. Thick films or 'paper' of 1T MoS₂ can be fabricated easily using a simple filtration technique to restack the suspended nanosheets (Fig. 1a–e). After exfoliation, the nanosheets are rigorously cleaned with hexane and deionized water to completely remove residual organolithium contamination (see Methods and Experimental Section in Supplementary Information and ref. 20 for details). We verified the structure and phases of the exfoliated nanosheets using high-resolution scanning transmission electron microscopy (STEM, Fig. 1f), X-ray diffraction (XRD, Fig. 1g) and X-ray photoelectron spectroscopy (XPS, Fig. 1h). The two polymorphs of monolayer MoS₂ can be identified by XPS from the Mo 3d and S 2p regions. It has been observed that the components from the 1T phase appear at a binding energy that is ∼0.9 eV lower than their 2H counterparts[20,21]. Deconvolution of the Mo 3d and S 2p regions of chemically exfoliated MoS₂ indicates that the 1T phase concentration of the nanosheets is ∼70%. In addition to the 1T content, examination of the Mo and S XPS peaks confirms the absence of oxidized Mo or S (Fig. 1h and Supplementary Fig. 1).

The XRD patterns (Fig. 1g) of bulk powder and restacked films of nanosheets reveal a broad (002) peak for restacked MoS₂. The (002) peak, attributed to the interplanar spacing between the nanosheets (6.15 Å), is the most intense, but a new (001) peak at $2\theta \approx 7.3°$ indicates an additional separation of 5.5–6 Å between the layers during restacking[22]. The broadness of the (002) peak and the presence of the (001) peak indicate that the nanosheets are randomly arranged during restacking, with large spacings between the layers. The surface area of the restacked films was found to be 9 m² g⁻¹ (ref. 11), which is substantially less than that found in carbons such as reduced graphene oxide[7,9,12]. We also confirmed that the restacked films of the 1T phase are hydrophilic and that the contact angle is <30° (Supplementary Fig. 4). In addition, it has been demonstrated that the 1T phase is stabilized by charge transfer from the butyl group of the organolithium exfoliation agent[23]. Our zeta potential measurements[24] (−40 to −50 mV) indicate that the nanosheets are negatively charged[23,24], which may also facilitate cation intercalation.

The high electrical conductivity (10–100 S cm⁻¹) of 1T phase MoS₂ allows the formation of reasonably thick films without any binding agent. The electrical conductivity of the 1T phase electrodes compares favourably with some of the best-performing reduced graphene oxide electrodes (∼100 S cm⁻¹) for supercapacitors[25]. Electrodes with thicknesses of up to 5 μm and area density of 2.5 mg cm⁻² were tested in this study. We first explored the electrochemical storage properties of the restacked MoS₂ films in 0.5 M H₂SO₄, Li₂SO₄, Na₂SO₄ and K₂SO₄ together with KCl and KBr electrolytes. The capacitance of the 1T phase MoS₂ electrodes was obtained using a standard three-electrode configuration in which saturated calomel and platinum served as the reference and counter electrodes, respectively. The resulting cyclic voltammograms (CVs) in H₂SO₄, Li₂SO₄, Na₂SO₄ and K₂SO₄ for potentials ranging from −0.15 V to 0.85 V versus NHE are shown in Fig. 2a.
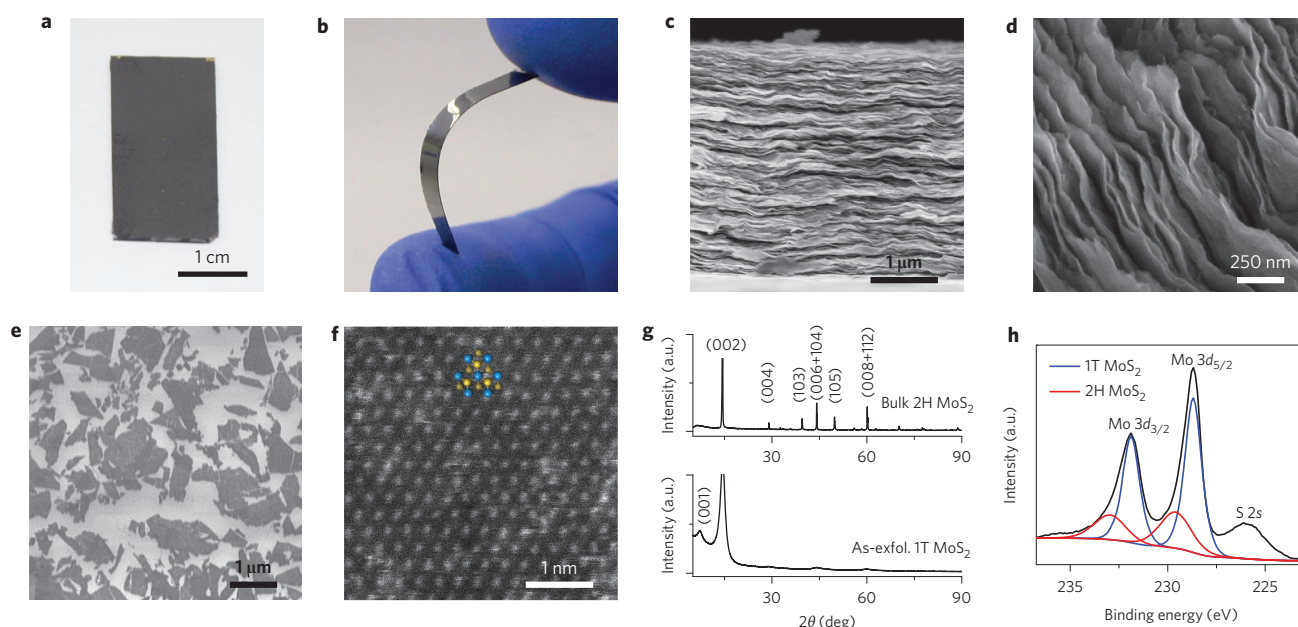
Materials Science and Engineering, 607 Taylor Road, Piscataway, New Jersey 08854, USA. *e-mail: manish1@rci.rutgers.edu

1

Figure 1 | Chemically exfoliated 1T MoS₂ electrodes. a,b, Photographs of electrodes consisting of a thick film of chemically exfoliated 1T MoS₂ prepared by vacuum filtration and transferred onto rigid glass (**a**) and a flexible polyimide substrate (**b**). **c,** Side view of the electrode observed by scanning electron microscopy (SEM) showing the layered nature of the film made by restacking exfoliated MoS₂ nanosheets. **d,** High-magnification image of restacked MoS₂ nanosheets. **e,** SEM image of as-exfoliated monolayer 1T phase MoS₂ nanosheets. **f,** High-angle annular dark-field scanning transmission electron microscope image of monolayer 1T phase MoS₂. Inset: Atomic structure of 1T phase MoS₂ (Mo and S atoms are displayed in blue and yellow, respectively). **g,** XRD of bulk MoS₂ compared with as-exfoliated restacked MoS₂. **h,** High-resolution X-ray photoelectron spectrum from the Mo 3d region of as-exfoliated 1T MoS₂ (black). Contributions from 1T and 2H phase components in the Mo 3d spectrum are indicated by blue and red curves, respectively.

The rectangular nature of the CV curves indicates capacitive behaviour of the electrodes. The deviation from rectangular behaviour for H_2SO_4 is attributed to electrosorption of protons on the surface of the nanosheets[14]. Typical CVs from 2H MoS₂ films under similar conditions in Na_2SO_4 are also shown for comparison. It can be clearly seen that the specific gravimetric capacitance increases by a factor of nearly 20 in the 1T phase electrodes. The specific gravimetric and volumetric capacitances were obtained from CV measurements (Supplementary page 8). The electrochemical impedance spectroscopy (EIS) data shown in Supplementary Fig. 8 show near-vertical curves for the different electrolytes, indicating close to ideal behaviour.

To elucidate whether the cations or anions intercalate into the electrodes, we tested two electrolytes with different anions. The CVs from K_2SO_4 and KCl are shown in Fig. 2b. It can be seen that, despite the large difference in anion radii, the CVs for both electrolytes are nearly the same, suggesting that it is the cation that is intercalating. The CVs plotted in Fig. 2c were obtained at scan rates ranging from 5 mV s⁻¹ to 1,000 mV s⁻¹ and show that the 1T electrodes retain their high capacitance values and rectangular shape, even at very high scan rates above 200 mV s⁻¹. A plot of specific capacitance versus scan rate for the different electrolytes tested in this study is shown in Fig. 2d. The high capacitance values at high scan rates may be explained by the fact that transition-metal chalcogenides possess higher ionic diffusivity due to their large anionic polarizability, which arises from the larger sizes of S^{2-} and Se^{2-} (ref. 26). It can be seen that the volumetric capacitance is dependent on the electrolyte, but shows exceptionally high values ranging from 400 to 650 F cm⁻³ at scan rates of 20 mV s⁻¹.

Galvanostatic charge/discharge measurements performed at 0.5, 1, 2, 4, 8 and 16 A g⁻¹ in Na_2SO_4 are shown in Fig. 2e. The curves show close to ideal triangular capacitive behaviour. We studied the cyclability of the electrodes by performing more than 5,000 charge/discharge cycles at a current rate of 2 A g⁻¹. Capacitive retention was

found to be greater than 93% in neutral electrolytes and greater than 97% in acidic electrolytes, as shown in Fig. 2f. XPS analysis of 1T phase MoS₂ electrodes conducted after 5,000 cycles did not show substantial change in the phase concentration. We also found coulombic efficiencies of 90–98% for various electrolytes at a charge/discharge current rate of 2 A g⁻¹.

To investigate the volumetric energy and power densities of 1T phase MoS₂ electrodes we measured their electrochemical storage properties in non-aqueous electrolytes. Specifically, we tested their properties in tetraethylammonium tetrafluoroborate (TEA BF_4)/MeCN and 1-ethyl-3-methylimidazolium tetrafluoroborate (EMIM BF_4)/MeCN organic electrolytes, because they offer a wide operating potential window of up to 3.5 V. For this phase of the study we used a two-electrode system as described in Supplementary pages 12–14. Figure 3a shows rectangular CVs for the measured scan rates in 1 M TEA BF_4 in acetonitrile with a 3 V potential range. As summarized in Fig. 3b, capacitances as high as 199 F cm⁻³ in TEA BF_4/MeCN and 250 F cm⁻³ in EMIM BF_4/MeCN were obtained from 1T MoS₂ electrodes at 5 mV s⁻¹. Galvanostatic charge/discharge measurements were conducted at current densities ranging from 0.5 A g⁻¹ to 32 A g⁻¹ (Fig. 3c). The charge/discharge curves show close to ideal behaviour with a minimal potential fall at higher discharging currents, as shown in the inset to Fig. 3c. The cyclic stability of the 1T phase electrodes in organic electrolytes was tested over 5,000 cycles (Fig. 2f). We found that the electrodes retained a capacitance in excess of 90% after 5,000 cycles. For 1T phase MoS₂ electrodes tested in aqueous electrolytes, we calculated an energy density of up to 0.016 Wh cm⁻³ at a current density of 0.5 A g⁻¹, giving a power density of 0.62 W cm⁻³. At 16 A g⁻¹, the energy and power densities reach 0.011 Wh cm⁻³ and 8.7 W cm⁻³, respectively. These values are dramatically increased in organic electrolytes. We found an energy density and power density as high as 0.11 Wh cm⁻³ and 1.1 W cm⁻³, respectively, at 0.5 A g⁻¹. At a higher current density of 32 A g⁻¹, these values change to 0.051 Wh cm⁻³ and 51 W cm⁻³. These energy and power densities
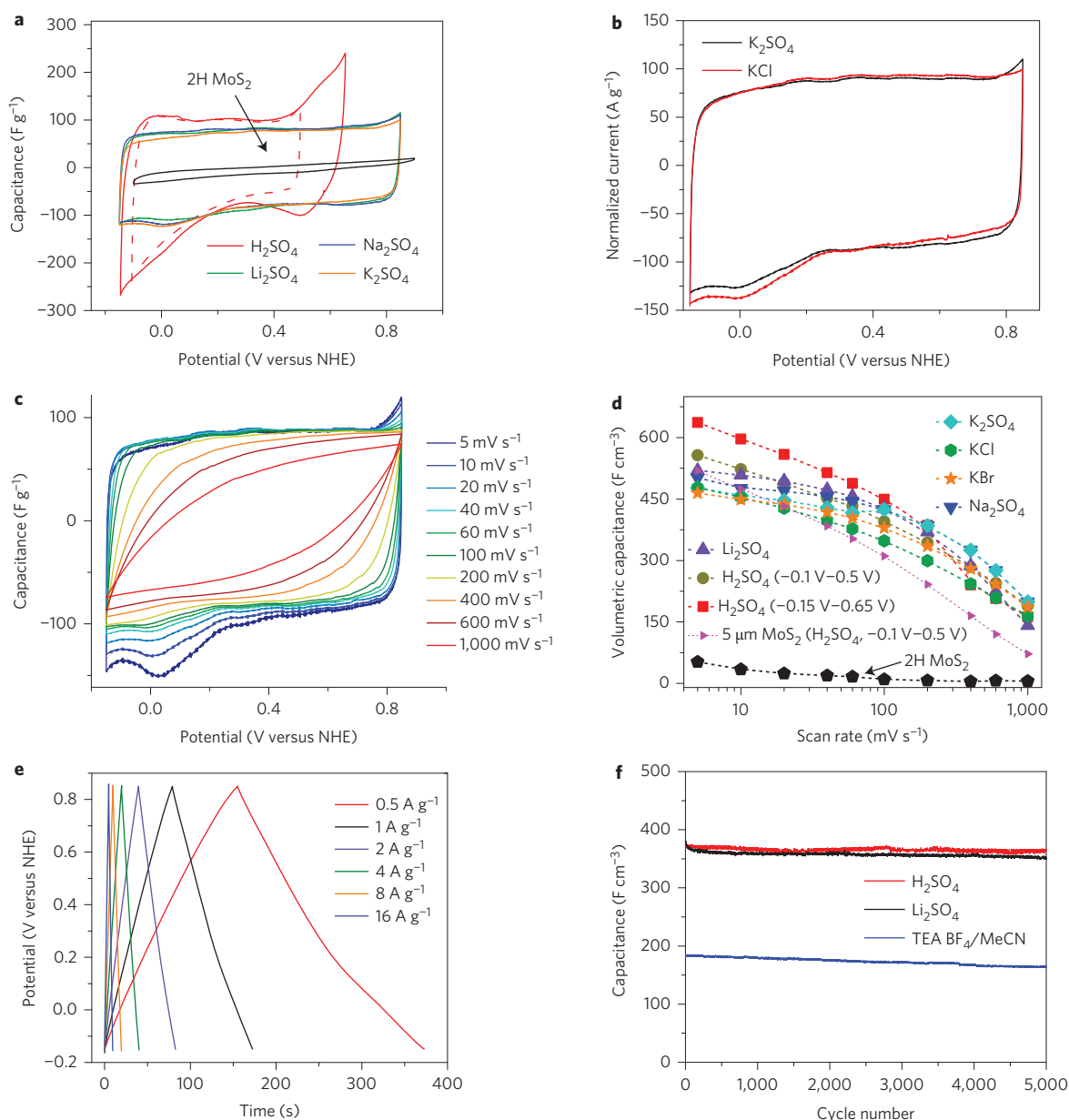
Figure 2 | Electrochemical characterization of 1T phase MoS$_2$ electrodes in different electrolytes. a, CVs of 1T phase MoS$_2$ nanosheet paper in 0.5 M sulphate-based electrolyte solutions at scan rates of 20 mV s^{-1}. **b**, Comparison of the CV curves of 1T MoS$_2$ in 0.5 M K$_2$SO$_4$ and 1 M KCl. The absence of a noticeable difference between the two electrolytes supports the fact that only cations are being stored. **c**, CVs of 1T phase MoS$_2$ electrodes in 0.5 M Na$_2$SO$_4$ from 5 mV s^{-1}–1,000 mV s^{-1}. The capacitance remains virtually constant up to scan rate of 100 mV s^{-1}. **d**, Evolution of the volumetric capacitance of the 1T phase MoS$_2$ electrodes with scan rate for different electrolytes and 1-μm- and 5-μm-thick films. The concentration of the cations in the electrolyte solutions was fixed at 1 M. **e**, Galvanostatic cycles from 0.5 A g^{-1}–16 A g^{-1} in K$_2$SO$_4$. **f**, Capacitance retention after 5,000 cycles in 0.5 M Li$_2$SO$_4$, H$_2$SO$_4$ and 1 M TEA BF$_4$ in acetonitrile.

are among the highest reported to date for a variety of electrode materials[8,12,13,27] (Fig. 3d), demonstrating the remarkable capacitive behaviour of 1T MoS$_2$ in both aqueous and organic electrolytes.

We performed XRD on intercalated electrodes to study the charge storage mechanism in 1T phase MoS$_2$ electrodes. *Ex situ* XRD spectra of electrodes intercalated with different cations and protons in neutral, acidic and organic electrolytes are shown in Fig. 4. As intercalation proceeds, the intensity of the (002) peak at 14.4° from restacked MoS$_2$ decreases, and the intensity of the (001) peak, which is an indication of interlayer expansion, increases. The new peak positions arising from expansion due to intercalation of cations or water are indicated in Fig. 4 as (001)* and (002)* peaks to differentiate them from those obtained in non-intercalated

materials. We note that the (001)* and (002)* peak positions strongly depend on the type of intercalant. The shoulder at ~16° indicated by the arrows for as-exfoliated MoS$_2$ and electrodes intercalated in Li$_2$SO$_4$, Na$_2$SO$_4$ and H$_2$SO$_4$ electrolytes is attributed to the presence of water bilayers[22]. Expansions of the spacing between the nanosheets due to intercalation are 6.63, 6.09, 3.7 and 4.83 Å for Li$_2$SO$_4$, Na$_2$SO$_4$, K$_2$SO$_4$ and TEA BF$_4$, respectively. These expansion values are higher than the hydrated cation sizes of Li$^+$(H$_2$O)$_2$, Na$^+$(H$_2$O)$_2$ and K$^+$(H$_2$O). The observed expansion values are consistent with previous XRD and NMR studies of MoS$_2$ intercalation compounds[22,28,29]. Interestingly, unlike neutral electrolytes, the (001) peak is absent after charging in H$_2$SO$_4$. This is attributed to the fact that smaller protons can easily
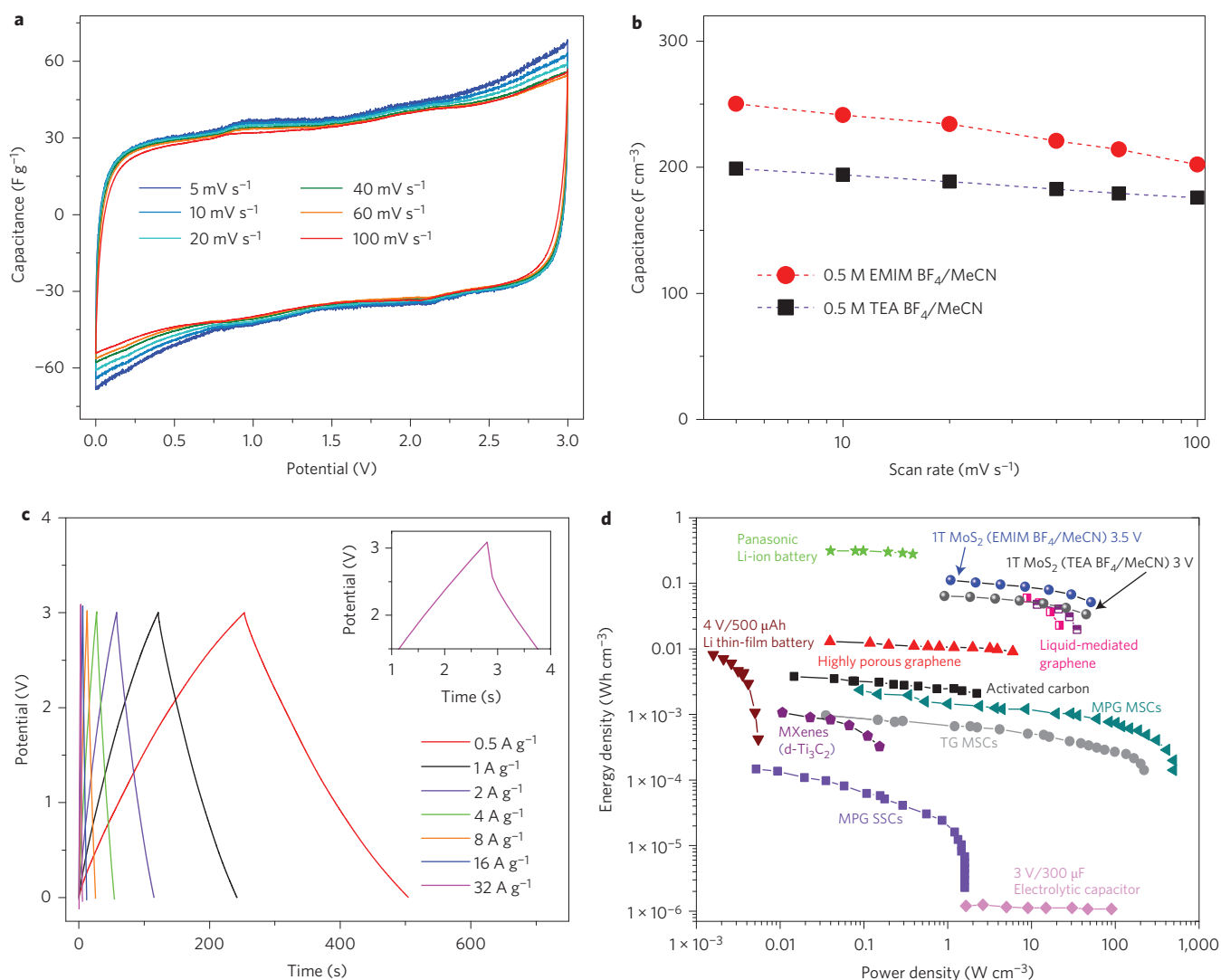
Figure 3 | Electrochemical behaviour of 1T phase MoS$_2$ electrodes in organic electrolytes. a, CVs in 1 M TEA BF$_4$/MeCN. **b**, Capacitance versus scan rate in TEA BF$_4$/MeCN and EMIM BF$_4$/MeCN electrolytes. **c**, Galvanostatic charge/discharge curves in TEA BF$_4$/MeCN at current rates from 0.5 A g^{-1} to 32 A g^{-1}. Inset: Low internal resistance of the 1T MoS$_2$ electrodes in 1 M TEA BF$_4$/MeCN at 32 A g^{-1}. **d**, Ragone plot of the best volumetric power and volumetric energy densities reported from various materials including lithium thin-film batteries[27], Panasonic Li-ion batteries[27], graphene[12,13,27] and MXenes[8] for comparison with those values obtained in this study for 1T phase MoS$_2$ electrodes. The Ragone plot consists of values calculated by taking into account the separator volume for lithium batteries, MXenes and liquid-mediated graphene, while the values for activated carbon, highly porous graphene and 1T phase MoS$_2$ were calculated from electrode volumes.

diffuse between the interlayer spacings in restacked MoS$_2$ without causing substantial expansion. However, a small shift is observed in the position of the (002) peak after proton intercalation in zero pH electrolytes. This can be related to adsorption on 1T phase MoS$_2$ after charging and is consistent with the shape of the CV curve in Fig. 2a. In the case of organic electrolytes, similar expansion has been observed with strong (001)* and (002)* peaks at 8° and 15.9°, as shown in Fig. 4(vi). The absence of (002) at 14.4° from restacked MoS$_2$ after intercalation in TEA BF$_4$/MeCN suggests that the 1T phase MoS$_2$ electrodes are fully intercalated with the organic electrolyte. The expansion of the interlayer spacings of the nanosheets suggests that the 1T phase MoS$_2$ electrodes dynamically expand to accommodate cations, despite the low surface area.

We have shown that exfoliated layers of the metallic 1T phase of MoS$_2$ have interesting electrochemical properties that can make it an attractive electrode material for both aqueous and organic supercapacitor devices. These electrochemical properties can be attributed to the intrinsic hydrophilicity and high electrical conductivity of 1T MoS$_2$, as well as the ability of the exfoliated nanosheets to intercalate various cations and the fact that our devices are devoid of binders and other additives. Following these results, we believe that other TMDs other than MoS$_2$ may exhibit favourable electrochemical properties, once a suitable metallic phase is chemically achieved.

References

1. Simon, P. & Gogotsi, Y. Materials for electrochemical capacitors. *Nature Mater.* **7,** 845–854 (2008).
2. Conway, B. E. Transition from 'supercapacitor' to 'battery' behavior in electrochemical energy storage. *J. Electrochem. Soc.* **138,** 1539 (1991).
3. Ghidiu, M., Lukatskaya, M. R., Zhao, M-Q., Gogotsi, Y. & Barsoum, M. W. Conductive two-dimensional titanium carbide 'clay' with high volumetric capacitance. *Nature* **516,** 78–81 (2014).
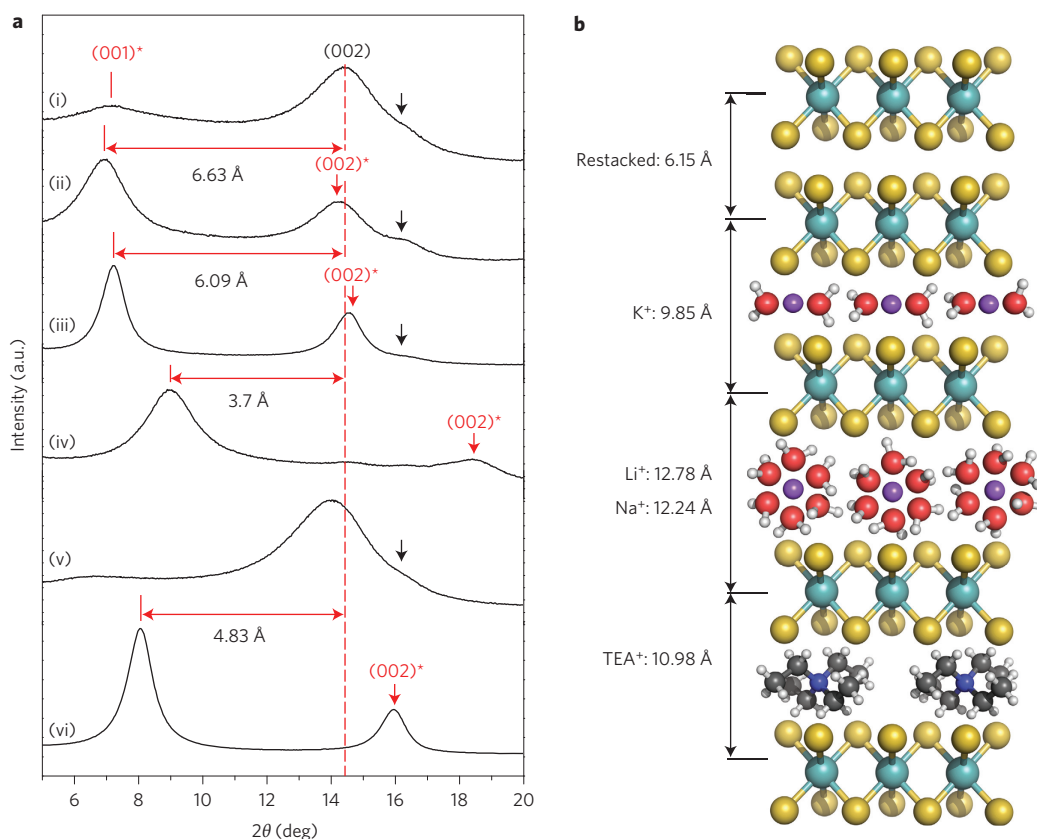
Figure 4 | *Ex situ* XRD spectra from restacked 1T phase MoS₂ films. a, XRD spectra from as-exfoliated 1T phase MoS_2 nanosheets (i) and cycled MoS_2 film (ii–vi) in different sulphate-based electrolytes: Li_2SO_4 (ii), Na_2SO_4 (iii), K_2SO_4 (iv), H_2SO_4 (v), and in TEA BF_4/MeCN organic electrolyte (vi). The characteristic (002) peak from restacked MoS_2 nanosheets is found at 14.4° for as-exfoliated 1T MoS_2. After intercalation, new peaks labelled (001)* and (002)* are detected indicating different spacing between the MoS_2 nanosheets. The presence of a shoulder at ~16° (black arrows) for as-exfoliated MoS_2 and electrodes intercalated in Li_2SO_4, Na_2SO_4 and H_2SO_4 electrolytes is attributed to the presence of water bilayers. **b**, Schematics of restacked non-intercalated and intercalated 1T MoS_2 nanosheets. Different spacings were measured by XRD depending on the hydrated intercalated ion. In the case of aqueous electrolyte, cations are coordinated with two water molecules for K^+ and six water molecules for Na^+ and Li^+. In organic electrolytes, the cations are desolvated during the intercalation process, giving a layer separation of 4.83 Å comparable to TEA^+ (3.85 Å; ref. 30).

4. Poizot, P., Laruelle, S., Grugeon, S., Dupont, L. & Tarascon, J-M. Nano-sized transition-metal oxides as negative-electrode materials for lithium-ion batteries. *Nature* **407**, 496–499 (2000).

5. Yoo, E. *et al.* Large reversible Li storage of graphene nanosheet families for use in rechargeable lithium ion batteries. *Nano Lett.* **8**, 2277–2282 (2008).

6. Mai, L. *et al.* Fast ionic diffusion-enabled nanoflake electrode by spontaneous electrochemical pre-intercalation for high-performance supercapacitor. *Sci. Rep.* **3**, 1718 (2013).

7. Stoller, M. D., Park, S., Zhu, Y., An, J. & Ruoff, R. S. Graphene-based ultracapacitors. *Nano Lett.* **8**, 3498–3502 (2008).

8. Lukatskaya, M. R. *et al.* Cation intercalation and high volumetric capacitance of two-dimensional titanium carbide. *Science* **341**, 1502–1505 (2013).

9. Zhu, Y. *et al.* Carbon-based supercapacitors produced by activation of graphene. *Science* **332**, 1537–1541 (2011).

10. Feng, J. *et al.* Metallic few-layered VS₂ ultrathin nanosheets: high two-dimensional conductivity for in-plane supercapacitors. *J. Am. Chem. Soc.* **133**, 17832–17838 (2011).

11. Du, G. *et al.* Superior stability and high capacity of restacked molybdenum disulfide as anode material for lithium ion batteries. *Chem. Commun.* **46**, 1106 (2010).

12. Tao, Y. *et al.* Towards ultrahigh volumetric capacitance: graphene derived highly dense but porous carbons for supercapacitors. *Sci. Rep.* **3**, 2975 (2013).

13. Yang, X., Cheng, C., Wang, Y., Qiu, L. & Li, D. Liquid-mediated dense integration of graphene materials for compact capacitive energy storage. *Science* **341**, 534–537 (2013).

14. Soon, J. M. & Loh, K. P. Electrochemical double-layer capacitance of MoS₂ nanowall films. *Electrochem. Solid-State Lett.* **10**, A250 (2007).

15. Cao, L. *et al.* Direct laser-patterned micro-supercapacitors from paintable MoS₂ films. *Small* **9**, 2905–2910 (2013).

16. Da Silveira Firmiano, E. G. *et al.* Supercapacitor electrodes obtained by directly bonding 2D MoS₂ on reduced graphene oxide. *Adv. Energy Mater.* **4**, 1301380 (2014).

17. Huang, K-J. *et al.* Synthesis of polyaniline/2-dimensional graphene analog MoS₂ composites for high-performance supercapacitor. *Electrochim. Acta* **109**, 587–594 (2013).

18. Ramadoss, A., Kim, T., Kim, G-S. & Kim, S. J. Enhanced activity of a hydrothermally synthesized mesoporous MoS₂ nanostructure for high performance supercapacitor applications. *New J. Chem.* **38**, 2379 (2014).

19. Splendiani, A. *et al.* Emerging photoluminescence in monolayer MoS₂. *Nano Lett.* **10**, 1271–1275 (2010).

20. Eda, G. *et al.* Photoluminescence from chemically exfoliated MoS₂. *Nano Lett.* **11**, 5111–5116 (2011).

21. Papageorgopoulos, C. A. & Jaegermann, W. Li intercalation across and along the van der Waals surfaces of MoS₂(0001). *Surf. Sci.* **338**, 83–93 (1995).

22. Joensen, P., Crozier, E. D., Alberding, N. & Frindt, R. F. A study of single-layer and restacked MoS₂ by X-ray diffraction and X-ray absorption spectroscopy. *J. Phys. C* **20**, 4043–4053 (1987).

23. Heising, J. & Kanatzidis, M. G. Exfoliated and restacked MoS₂ and WS₂: ionic or neutral species? encapsulation and ordering of hard electropositive cations. *J. Am. Chem. Soc.* **121**, 11720–11732 (1999).

24. Voiry, D. *et al.* Conducting MoS₂ nanosheets as catalysts for hydrogen evolution reaction. *Nano Lett.* **13**, 6222–6227 (2013).

25. Zhu, Y. *et al.* Graphene and graphene oxide: synthesis, properties, and applications. *Adv. Mater.* **22**, 3906–3924 (2010).

26. Zheng, N., Bu, X. & Feng, P. Synthetic design of crystalline inorganic chalcogenides exhibiting fast-ion conductivity. *Nature* **426**, 428–432 (2003).

27. Wu, Z., Parvez, K., Feng, X. & Müllen, K. Graphene-based in-plane micro-supercapacitors with high power and energy densities. *Nature Commun.* **4**, 2487 (2013).

28. Schöllhorn, R. & Weiss, A. Cation exchange reactions and layer solvate complexes of ternary phases M_xMoS_2. *J. Common Met.* **36,** 229–236 (1974).
29. Alexiev, V., Meyer zu Altenschildesche, H., Prins, R. & Weber, T. Solid-state NMR study of hydrated intercalation compounds of molybdenum disulfide. *Chem. Mater.* **11,** 1742–1746 (1999).
30. Palomo, J. Competitive absorption of quaternary ammonium and alkali metal cations into a Nafion cation-exchange membrane. *J. Membr. Sci.* **215,** 103–114 (2003).

Acknowledgements

Author contributions

M.C. and M.A. conceived the idea and designed the experiments. M.A. synthesized the materials, carried out the electrochemical measurements, performed XRD analyses and assisted D.V. with XPS. D.V. assisted in materials synthesis, and performed Raman, XPS and SEM measurements. M.C. wrote the manuscript with assistance from M.A. and D.V. All authors discussed the results and commented on the manuscript.

Additional information

Supplementary information is available in the online version of the paper. Reprints and permissions information is available online at www.nature.com/reprints. Correspondence and requests for materials should be addressed to M.C.

Competing financial interests

The authors declare no competing financial interests.